ELSEVIER

J. Non-Newtonian Fluid Mech. 130 (2005) 96–109

Journal of Non-Newtonian Fluid Mechanics

www.elsevier.com/locate/jnnfm

Forward roll coating flows of viscoelastic liquids

G.A. Zevallos [a], M.S. Carvalho [a,*], M. Pasquali [b,**]

[a] *Department of Mechanical Engineering, Pontificia Universidade Catolica do Rio de Janeiro, Rua Marques de Sao Vicente 225, Gavea, Rio de Janeiro, RJ 22453-900, Brazil*

[b] *Department of Chemical & Biomolecular Engineering, Rice University, MS 362, 6100 Main St., Houston, TX 77005, USA*

Received 10 September 2004; received in revised form 23 July 2005

Abstract

Roll coating is distinguished by the use of one or more gaps between rotating cylinders to meter and apply a liquid layer to a substrate. Except at low speed, the two-dimensional film splitting flow that occurs in forward roll coating is unstable; a three-dimensional steady flow sets in, resulting in more or less regular stripes in the machine direction. For Newtonian liquids, the stability of the two-dimensional flow is determined by the competition of capillary and viscous forces: the onset of meniscus nonuniformity is marked by a critical value of the capillary number. Although most of the liquids coated industrially are non-Newtonian polymeric solutions and dispersions, most of the theoretical analyses of film splitting flows relied on the Newtonian model. Non-Newtonian behavior can drastically change the nature of the flow near the free surface; when minute amounts of flexible polymer are present, the onset of the three-dimensional instability occurs at much lower speeds than in the Newtonian case.

Forward roll coating flow is analyzed here with two differential constitutive models, the Oldroyd-B and the FENE-P equations. The results show that the elastic stresses change the flow near the film splitting meniscus by reducing and eventually eliminating the recirculation present at low capillary number. When the recirculation disappears, the difference of the tangential and normal stresses (i.e., the hoop stress) at the free surface becomes positive and grows dramatically with fluid elasticity, which explains how viscoelasticity destabilizes the flow in terms of the analysis of Graham [M.D. Graham, Interfacial hoop stress and instability of viscoelastic free surface flows, Phys. Fluids 15 (2003) 1702–1710].

Keywords: Roll coating; Viscoelastic flow; Free surface; Instability; Finite element

1. Introduction

Roll coating is widely used to apply a thin liquid layer to a continuous, flexible substrate. At low speeds the flow is two-dimensional and steady; as the roll speed is raised, the two-dimensional flow becomes unstable and is replaced by a steady three-dimensional flow which results in more or less regular stripes in the machine direction (Fig. 1). This type of instability, or rather the three-dimensional flow to which it may lead, is commonly called *ribbing*; it can limit the speed of the process if a smooth film is required as a final product.

The film-splitting flow of a Newtonian liquid exiting from two rotating rolls and the associated instability have been studied extensively. Pearson [2] was the first to analyze why a flow that otherwise leads to a uniform meniscus can turn unstable. He showed that the adverse pressure gradient near the film-split meniscus necessary to decelerate the flowing liquid destabilizes the free surface, whereas surface tension has a stabilizing effect. A critical value of the ratio between these two forces, i.e., the capillary number $Ca \equiv \mu V/\varsigma$, marks the onset of the free surface nonuniformity. Here, μ is the liquid viscosity, ς its surface tension, and V is the mean roll speed. Further experiments and theoretical models to describe the film-splitting instability of Newtonian liquids between rigid rolls have been developed in refs. [3–8].

In practice, coating liquids often contain polymers. Non-Newtonian behavior can drastically change the nature of the flow near the free surface and consequently alter the performance of a coater. The first analyses of non-Newtonian effects in roll coating flows were restricted to shear-thinning behavior and simple power-law models. By solving the two-dimensional conservation equations of a shear-sensitive liquid, Coyle et al. [9] showed the effect of shear-thinning on the film thickness and pressure distribution along the coating bead. Bauman et al. [10] experimentally tested the effect of certain polymer additives on the

* Corresponding author. Fax: +55 21 3114 1165.

** Corresponding author. Fax: +1 713 348 5478.

E-mail addresses: msc@mec.puc-rio.br (M.S. Carvalho), mp@rice.edu (M. Pasquali).

0377-0257/$ – see front matter © 2005 Elsevier B.V. All rights reserved.
doi:10.1016/j.jnnfm.2005.08.005

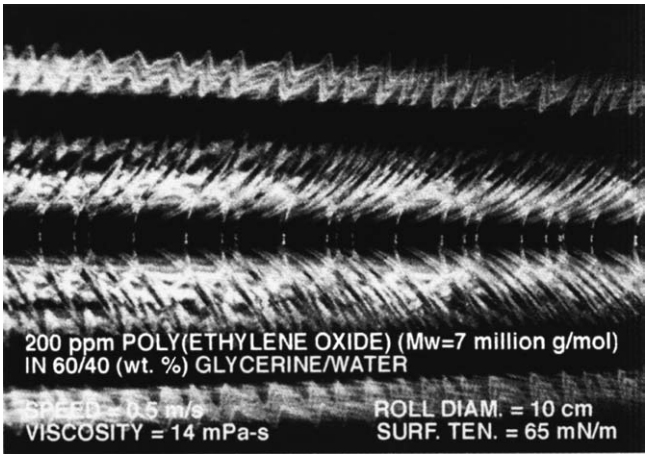

Fig. 1. Three-dimensional periodic flow in forward roll coating film splitting (from [17]).

ribbing instability. They observed that the critical speed at which ribbing first appeared was lower than in the case of a Newtonian liquid. They advanced simple arguments about the effect of liquid elasticity on the stability of the flow. They concluded that the elastic stresses that appears in the extensional flow near the free surface destabilize the flow. The formation of small liquid drops at the film split meniscus, a phenomenon known as spatter and misting, was studied by Glass [11–14]. He observed roll spatter in coating of aqueous dispersions of colloidal polymer plus other ingredients in 'latex' paints by evaluating several trade paints and comparing their propensity to spatter. Their main conclusion was that paints with high apparent extensional viscosity produced large and stable filaments. Fernando and co-workers [15,16] addressed spattering in commercial paints. They found that the instability occurred at lower capillary number in liquids with higher apparent extensional viscosity (measured by fiber-suction technique). Moreover, the length of filaments and the intensity of misting increased with the apparent extensional viscosity. Carvalho et al. [17], and later Dontula [18], analyzed experimentally the film splitting flow of aqueous solutions of PEG and PEO. They concluded that minute amounts of flexible polymer lowered drastically the critical speed at which the three-dimensional instability occurs. Grillet et al. [19] and recently Lopez et al. [20] studied experimentally the instability of non-Newtonian flow between two non-concentric cylinders. The latter used two aqueous polymer solutions with similar shear-thinning behavior but different elastic characteristics, i.e., xanthan (inelastic) and polyacrylamide (elastic). With the elastic (polyacrylamide) solution, the critical capillary number for the instability dropped with growing polymer concentration by up to one order of magnitude compared to the Newtonian case. With the xanthan solution, the critical capillary number decreased only slightly. The resulting three-dimensional pattern of the free surface is also a strong function of the liquid properties, which suggests that the instability mechanism may be different in the case of viscoelastic liquids.

Accurate theoretical predictions of the onset of ribbing when viscoelastic liquids are used is still not available. The mechanisms by which the liquid elasticity makes the flow unstable at capillary numbers much lower than in the Newtonian case is not completely understood.

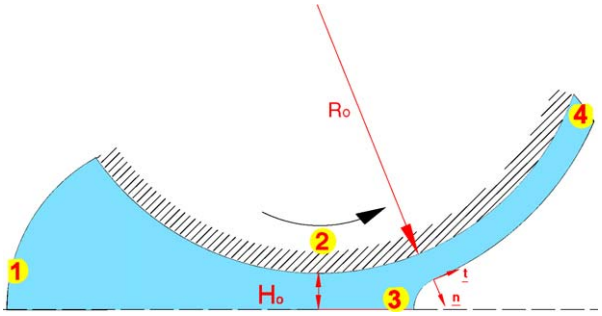

Fig. 2. Sketch of instability mechanisms proposed by Pitts and Greiller, and Graham.

The stability problem can be approached in two ways: (1) by analyzing the two-dimensional flow kinematics at the free surface and extracting simple criteria to estimate the critical capillary number and (2) by computing the two-dimensional flow by solving the mass and momentum balance equations together with a suitable constitutive equation for the stress, and then assessing the stability of this flow to infinitesimal three-dimensional perturbations.

Simple criteria to estimate the stability of film splitting flows have been proposed for Newtonian liquids by Pitts and Greiller [3] and for viscoelastic liquids by Graham [1].

The stability criterion proposed by Pitts and Greiller [3] is based on a spanwise momentum balance along the perturbed free surface. In this analysis, the viscous (and viscoelastic) stresses are neglected and only the pressure is considered as the driving force for the instability. The flow is considered unstable if the transverse normal tensile stress under the perturbed free surface at the midpoint between the crest and the throat of the developing wave (location 1 in Fig. 2) is smaller than the transverse normal stress at the same streamwise location beneath the crest of the wave (location 2 in Fig. 2)—or, conversely, if the pressure beneath the crest of the wave (location 3 in Fig. 2) is higher than that at the midpoint between the crest and the throat (location 1 in Fig. 2). In this case, the gradient of spanwise stress will drive flow from the throat into the crest of the wave and thus the instability will grow. The flow is stable if

$$-\frac{\mathrm{d}p}{\mathrm{d}r} < \varsigma\left(\frac{\mathrm{d}\mathcal{H}}{\mathrm{d}r} + N^2\right), \tag{1}$$

where $\mathcal{H} \equiv 1/\mathcal{R}$ is the in-plane curvature of the film splitting meniscus, ς is the liquid surface tension, r is a coordinate along the normal to the free surface (see Fig. 2), and N is the wavenumber of the perturbation. Of course, this simple criterion does not predict correctly the wavenumber of the instability, but it identifies correctly the competition of the relevant forces. Based on this analysis, Pitts and Greiller [3] estimated that the critical capillary number at the onset of ribbing is a function of the ratio of the gap between the rolls $2H_0$ to the roll radius R, and ought to be

$$Ca^* = 28\frac{H_0}{R}. \tag{2}$$

Recently, Graham [1] proposed a different simplified criterion to asses the stability of a flow under a curved free surface. The key, novel component of Graham's analysis is the introduction of a local cylindrical coordinate system at the free surface which allows the incorporation of the normal stress difference at the free surface on the radial component of the momentum balance equation. The combination of a large normal stress difference, i.e., "hoop stress", and curvature along a concave free surface destabilizes the flow. A perturbation theory was presented to show that a disturbance that locally thickens the liquid layer enhances the normal stress difference at that location, which drives further thickening of the liquid layer. Capillary forces counteract this tendency and stabilize the flow. According to Graham's criterion, the flow is stable when

$$\frac{\mathrm{d}T_{rr}}{\mathrm{d}r} - \rho g_r = \mathcal{H}(\sigma_{\theta\theta} - \sigma_{rr}) - \rho g_r < \varsigma N^2. \tag{3}$$

However, this analysis neglects an important term present in the earlier work of Pitts and Greiller [3], namely the stabilizing effect of meniscus curvature variation at the separating stagnation point due to free surface position variation, i.e., $\varsigma(\mathrm{d}\mathcal{H}/\mathrm{d}r)$—this term was present in an earlier analysis by Graham [21]. Whereas this term is irrelevant in flows where the free surface develops between nearly parallel plates (such as planar Hele–Shaw flow, for example), it is important in flows between diverging surfaces, such as roll coating flows, because it accounts for the effect of an outward motion of the free surface which stabilizes the flow because it reduces the capillary pressure drop across the free surface and thus diminishes the pressure gradient beneath the free surface. The complete (simplified) criterion is

$$\frac{\mathrm{d}T_{rr}}{\mathrm{d}r} - \rho g_r = \mathcal{H}(\sigma_{\theta\theta} - \sigma_{rr}) - \rho g_r < \left(\frac{\mathrm{d}\mathcal{H}}{\mathrm{d}r} + N^2\right); \tag{4}$$

it reduces to Pitts and Greiller's criterion (Eq. (1)) if viscous forces are neglected ($T_{rr} = -p$).

Scriven and co-workers [8,22,23] analyzed the stability problem more rigorously in the case of various Newtonian coating flows by evaluating the response of the two-dimensional, steady-state flow to infinitesimal periodic disturbances. Such linear stability analysis was used successfully to determine critical capillary numbers at different gap to roll ratio at the onset of ribbing for both rigid and deformable forward roll coating flows of Newtonian liquids.

Modeling of viscoelastic coating flows must rely on theories that can capture sufficiently well the interplay of flow and liquid microstructure. Moreover, coating flows always involve free surfaces; the domain where the differential equations are posed is unknown a priori and it is part of the solution, and the shape of the free surfaces must be captured well because capillarity is one of the key forces that control the flow. These two characteristics make the problem extremely complex, and prototypical steady viscoelastic free surface coating flows have been studied only recently [24–27]. Likewise, the stability analysis of viscoelastic flows is fraught with difficulties. Simple non-viscometric flows have been tacked successfully recently [28,29], and methods for linear stability analysis of viscoelastic free surface flows are still under investigation.

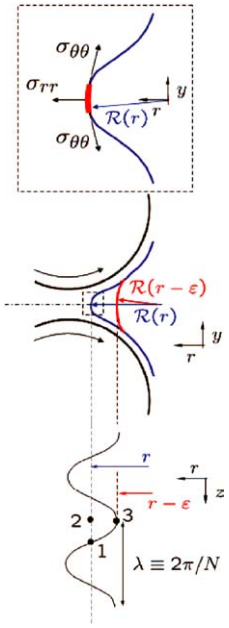

Fig. 3. Sketch of a forward roll coating bead. Domain at which the conservation equations are solved.

In this work, the two-dimensional, viscoelastic, free surface roll coating flow is analyzed with two differential constitutive models: the Oldroyd-B and the FENE-P equations. The free boundary problem is transformed into a fixed boundary problem by mapping the unknown domain into a reference one [25,30–33], and the continuity, momentum, conformation, and mesh mapping equations are solved with the DEVSS-TG/SUPG method with finite element basis functions [25].

The computed flow and stress fields are analyzed in light of Graham's [1] work to understand the role of the elastic stress on the force balance at the interface and how liquid elasticity destabilizes the two-dimensional flow.

2. Mathematical model

The flow domain where the governing equations are integrated is sketched in Fig. 3. The two rolls are moving from left to right in the figure at equal speed V. The minimum clearance between the rolls is $2H_0$. The position of the meniscus is unknown a priori and it is a function of the liquid properties and operating conditions.

2.1. Governing equations

For incompressible and isothermal flow, the momentum and continuity equations are:

$$\rho\mathbf{v}\cdot\nabla\mathbf{v} - \nabla\cdot\mathbf{T} = \mathbf{0} \quad \text{and} \quad \nabla\cdot\mathbf{v} = 0 \tag{5}$$

where ρ is the liquid density and $\mathbf{T} \equiv -p\mathbf{I} + \tau + \boldsymbol{\sigma}$ is the total stress tensor, the sum of pressure p, viscous stress $\tau \equiv 2\eta_s\mathbf{D}$ and elastic stress $\boldsymbol{\sigma}$, where η_s is the solvent viscosity and $\mathbf{D}$ is the rate of strain tensor.

The viscoelastic liquid is modeled by introducing the conformation dyadic $\mathbf{M}$, which represents the stretch and orientation of

Table 1
Constitutive parameters of the Oldroyd-B and FENE-P models

Constitutive model	ξ	ζ	g_0	g_1	g_2	$a(\mathbf{M})$
Oldroyd-B	1	1	−1	1	0	$G/(2\mathrm{tr}\mathbf{M})$
FENE-P	1	1	−1	$(b-1)/(b-\mathrm{tr}\mathbf{M}/3)$	0	$(3/2)G(b-1)\ln[(b-1)/(b-\mathrm{tr}\mathbf{M}/3)]$

Note that in the FENE-P model, the function $g_1 = 1$ at equilibrium ($\mathbf{M} = \mathbf{I}$); thus, the definitions of relaxation time and b differ slightly from those in ref. [38].

the flowing polymer molecules [34–36]. The equation of change of conformation can be written as [25,36]

$$\frac{\partial \mathbf{M}}{\partial t} + \mathbf{v}\cdot\nabla\mathbf{M} - 2\xi\frac{\mathbf{D}:\mathbf{M}}{\mathbf{I}:\mathbf{M}}\mathbf{M} - \zeta\left(\mathbf{M}\cdot\mathbf{D} + \mathbf{D}\cdot\mathbf{M} - 2\frac{\mathbf{D}:\mathbf{M}}{\mathbf{I}:\mathbf{M}}\mathbf{M}\right) - \mathbf{M}\cdot\mathbf{W} - \mathbf{W}^{\mathrm{T}}\cdot\mathbf{M} + \frac{1}{\lambda}(g_0\mathbf{I} + g_1\mathbf{M} + g_2\mathbf{M}^2) = 0 \quad (6)$$

where $\mathbf{W}$ is the vorticity tensor, λ the characteristic relaxation time of the polymer, $\xi(\mathbf{M})$ and $\zeta(\mathbf{M})$ represent the resistance to stretching and relative rotation of polymer segments, and $g_0(\mathbf{M})$, $g_1(\mathbf{M})$ and $g_2(\mathbf{M})$ define the rate of relaxation of the polymer segments. Different constitutive models can be obtained by specifying the appropriate form of the constitutive functions ξ, ζ, g_0, g_1 and g_2 (see refs. [34–37] for summary tables).

The relationship between elastic stress and conformation is [34,36]:

$$\hat{\boldsymbol{\sigma}} = 2(\xi-\zeta)\frac{\mathbf{M}}{\mathbf{I}:\mathbf{M}}\mathbf{M} : \frac{\partial a}{\partial \mathbf{M}} + 2\zeta\mathbf{M}\cdot\frac{\partial a}{\partial \mathbf{M}} \quad (7)$$

where $a(T, \mathbf{M})$ is the Helmholtz free energy per unit volume. Because the liquid is incompressible, the isotropic part of the elastic stress is constitutively indeterminate [36]; in order to keep the same meaning of the pressure term in the momentum balance equation, the elastic stress is constructed so as to be traceless,

$$\boldsymbol{\sigma} = \hat{\boldsymbol{\sigma}} - \frac{\mathrm{tr}\hat{\boldsymbol{\sigma}}}{\mathrm{tr}\mathbf{I}}\mathbf{I} \quad (8)$$

so that in both Newtonian and viscoelastic liquids the pressure coincides with the mechanical pressure $p \equiv -\mathrm{tr}(\mathbf{T})/3$.

Two different constitutive models—Oldroyld-B and FENE-P [38]—are used in this work. Both models assume that the molecules follow imposed large-scale deformation affinely. In the first, the rate of relaxation of the molecules is a linear function of the distance of the conformation tensor $\mathbf{M}$ from its equilibrium value $\mathbf{I}$. In the second, the maximum extension of the molecules is finite, and their rate of relaxation grows without bound as the average molecular extension approaches its maximum value. Table 1 reports the constitutive functions and the free energy for each model.

Thus, the constitutive parameters are: the polymer elastic modulus G, the relaxation time λ, and the ratio of the maximum length square of the polymer molecules to their average length square at equilibrium b (only for FENE-P). In both models, the polymer viscosity η_{p} can be defined as a function of the elastic modulus and relaxation time, i.e., $\eta_{\mathrm{p}} = G\lambda$.

The boundary conditions are:

(1) *Inflow: flooded condition and fully developed conformation tensor.*

The flow in a forward roll coating gap is self-metering, i.e. the flow rate is not known a priori. A pressure datum $p = P_0 = 0$ is imposed at the inflow boundary. The inflow boundary is located far upstream of the nip, so that there the conformation of the polymer molecules does not change along streamlines, i.e., $\mathbf{v}\cdot\nabla\mathbf{M} \approx 0$. Consequently, at the inflow boundary ($\mathbf{n}\cdot\mathbf{v} < 0$) the following algebraic equation is imposed [39]:

$$-2\xi\frac{\mathbf{D}:\mathbf{M}}{\mathbf{I}:\mathbf{M}}\mathbf{M} - \zeta\left(\mathbf{M}\cdot\mathbf{D} + \mathbf{D}\cdot\mathbf{M} - 2\frac{\mathbf{D}:\mathbf{M}}{\mathbf{I}:\mathbf{M}}\mathbf{M}\right) - \mathbf{M}\cdot\mathbf{W} - \mathbf{W}^{\mathrm{T}}\cdot\mathbf{M} + \frac{1}{\lambda}(g_0\mathbf{I} + g_1\mathbf{M} + g_2\mathbf{M}^2) = 0 \quad (9)$$

(2) *Roll surfaces: no-slip, no-penetration.* $\mathbf{v} = \Omega R\mathbf{t} = V\mathbf{t}$, where R is the roll radius, Ω the angular speed of the rolls, and $\mathbf{t}$ is the unit tangent vector to the roll surface in the direction of rotation.

(3) *Free surface: force balance and kinematic condition.*

$$\mathbf{n}\cdot\mathbf{T} = \varsigma\frac{\mathrm{d}\mathbf{t}}{\mathrm{d}s} - \mathbf{n}P_{\mathrm{amb}} \quad \text{and} \quad \mathbf{n}\cdot\mathbf{v} = 0 \quad (10)$$

ς is the liquid surface tension, s the coordinate along the free surface, and P_{amb} is the ambient pressure. It is set to zero.

(4) *Outflow: fully developed flow.* $\mathbf{n}\cdot\nabla\mathbf{v} = 0$ (refs. [39,40] for details).

2.2. Solution method

Because of the free surfaces, the flow domain is unknown a priori. Capillarity is comparable to viscous and elastic forces in coating flows; fully coupled solution methods (where the domain shape and the flow solution are computed simultaneously) are superior to loosely-coupled method (where the domain shape and the flow are computed alternatively in a fixed-point iteration scheme). Fully coupled methods rely on mapping the unknown physical domain Ω into a known reference domain Ω_0 by means of a bijective transformation $\mathbf{x} = \mathbf{x}(\xi)$, where $\mathbf{x}$ and ξ denote position in the physical and reference domain, respectively [30–32,41–45]. The mapping used here is governed by elliptic equations [25,32,46]

$$\nabla\cdot(\tilde{\mathbf{D}}\cdot\nabla\xi) = 0 \quad (11)$$

where $\tilde{\mathbf{D}}$ is a symmetric positive definite tensor of diffusion-like coefficients used to control element spacing. Boundary conditions are needed in order to solve the second-order partial differ-

ential equations (11). Along solid walls and synthetic inlet and outlet planes, the boundary is located by imposing a relation between the coordinates from the equation that describes the shape of the boundary, and stretching functions are used to distribute the points along the boundaries. The free boundary (gas–liquid interface) is located by imposing the kinematic condition (10).

The set of differential equations that describe the conservation of momentum and mass (5), the evolution of the polymer conformation (6), and define the mapping between the physical and reference domain (11), together with the algebraic equations for the viscous and elastic stresses are all solved on the reference domain Ω_0 by the finite element method. The formulation used here is the DEVSS-TG/SUPG [24,25], a modification of the DEVSS-G/SUPG finite element method [47,48] where the continuous representation of the velocity gradient field is traceless by definition, $\mathbf{L} - \nabla\mathbf{v} + (\nabla \cdot \mathbf{v})\mathbf{I}/(\mathrm{tr}\mathbf{I}) = 0$.

The position and velocity fields are represented by Lagrangian biquadratic basis functions, the pressure field by linear discontinuous basis functions and the interpolated velocity gradient and the conformation tensor by Lagrangian bilinear basis functions. The mesh generation equations and the momentum equation are weighted with Lagrangian biquadratic basis functions (Galerkin), the continuity equation with linear discontinuous (Galerkin), and the velocity gradient interpolation with Lagrangian bilinear (Galerkin). The conformation transport equation is weighted with the Streamline–Upwind Petrov–Galerkin method, $\psi_{\mathbf{M}} \equiv \varphi_{\mathbf{M}} + h^{\mathrm{u}}\mathbf{v} \cdot \nabla\varphi_{\mathbf{M}}$. The upwind parameter h^{u} coincides with the characteristic size of the smallest element in the finite element mesh.

The set of nonlinear algebraic equations that arises from applying the method of weighted residuals and the variables representation in terms of basis functions is solved by Newton's method with analytical Jacobian and first order arclength continuation [49,50] and a bordering algorithm [51]. Three different meshes were used. The main difference between them is the level of refinement near the free surface. Mesh 1 has 20 element across the film thickness and 60 elements along the film split free surface. The total number of degrees of freedom is 49,260. Mesh 2 has 30 elements across the film thickness and 90 elements along the free surface, resulting in a total number of degrees of freedom equal to 109,525. The finest mesh, Mesh 3, has 40 elements across the film thickness, 120 elements along the free surface and a total number of degrees of freedom equal to 193,548. Fig. 4 shows the tesselation near the free surface for Meshs 1 and 3.

3. Results

The important dimensionless parameters for the flow studied here are:

(1) Reynolds number: $Re = \rho VR/H_0 \equiv 0$ hereafter;
(2) Capillary number: $Ca = (\eta_{\mathrm{s}} + \eta_{\mathrm{p}})V/\varsigma$;
(3) Dimensionless gap: $H_0/R \equiv 0.01$ hereafter;
(4) Weissenberg number: $We = \lambda V/H_0$;
(5) Solvent to total viscosity ratio: $\beta = \eta_{\mathrm{s}}/(\eta_{\mathrm{s}} + \eta_{\mathrm{p}}) \equiv 0.59$ hereafter;
(6) Polymer molecules extensibility (when using FENE-P model): b.

3.1. Newtonian liquids

The variation of the predicted flow rate in units of roll speed times gap, and consequently the film thickness, with capillary number is small. It varies from $q \equiv Q/2VH_0 \simeq 1.34$ to $q \simeq 1.30$, in the range of capillary number explored here, e.g. $0.1 \leq Ca \leq 2$. Unlike in slot coating and Hele–Shaw flow between parallel walls, the film thickness is nearly independent of capillary number because at higher capillary number the location of the meniscus moves towards the minimum gap changing the curvature of the free surface. These results reproduce those

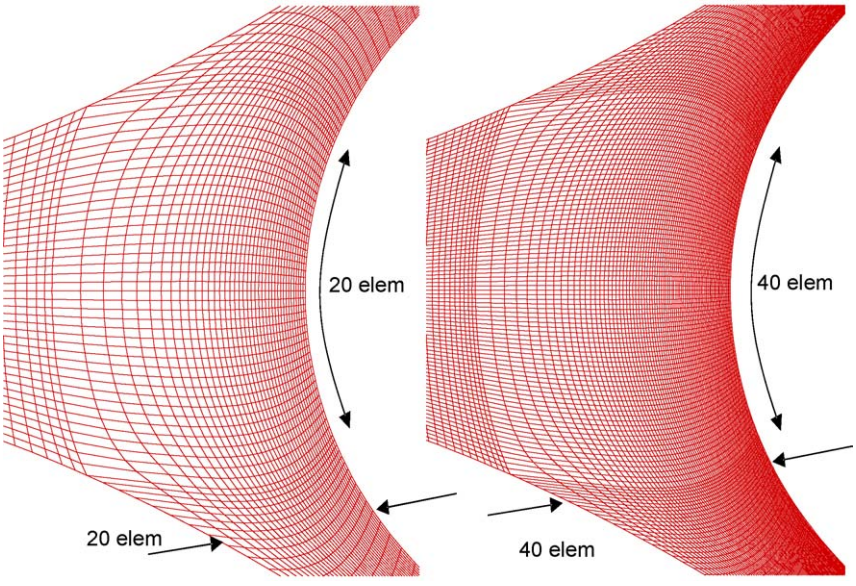

Fig. 4. Detail of Meshs 1 and 3 near the film splitting free surface.

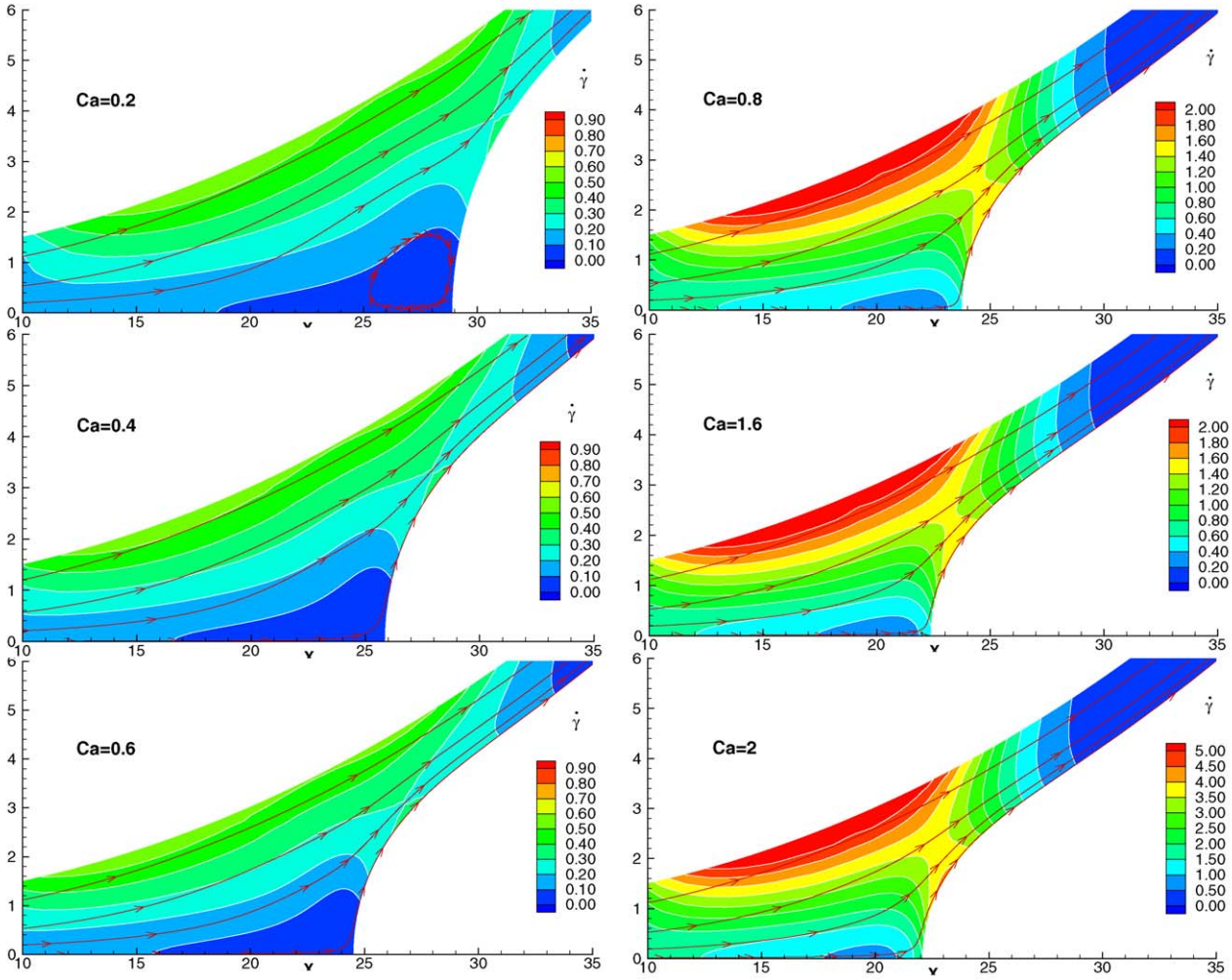

Fig. 5. Evolution of the streamlines and second invariant of the rate of deformation tensor as a function of capillary number for Newtonian flow.

presented by Coyle et al. [8]. The meniscus position is a strong function of the capillary number. If surface tension is strong compared to the viscous forces, i.e. at low capillary number, the meniscus is pulled away from the gap, the curvature of the free surface at the symmetry plane is small and a recirculation attached to the meniscus is present (Fig. 5). As the capillary number rises, the meniscus recedes and the free surface becomes more curved. Because the rolls are rotating at equal speed, the flow is symmetric and only half of the flow domain is shown. Above $Ca = 0.4$, no recirculation is present and there is only one stagnation point at the free surface, located at the mid-plane between the rolls. The evolution of the positive eigenvalue of the rate of strain tensor, in units of roll speed over half the distance between the rolls, is also shown in the plot. There is a region of large deformation rate near the roll surface. The deformation in this part of the flow is dominated by shear. Downstream of the stagnation point at the free surface, the liquid is accelerated to the roll speed, and a local maximum of the deformation rate at the free surface can be observed. The deformation in this part of the flow is dominated by extension. As the capillary number grows, the maximum deformation rate along the free surface rises and the position of the local maximum moves upstream.

At low capillary number, e.g. $Ca \leq 0.6$, the deformation rate along the symmetry line close to the meniscus is small and depends weakly on capillary number, even on flows that do not have a recirculation attached to the free surface ($Ca = 0.4$ and 0.6), as

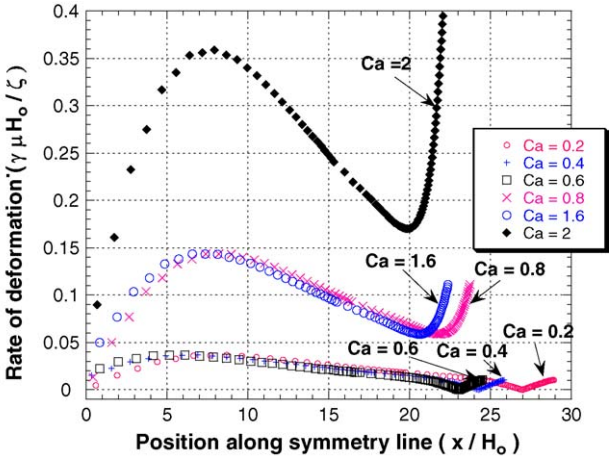

Fig. 6. Rate of deformation along the symmetry line at different capillary numbers. Each curve ends at the correspondent meniscus position.

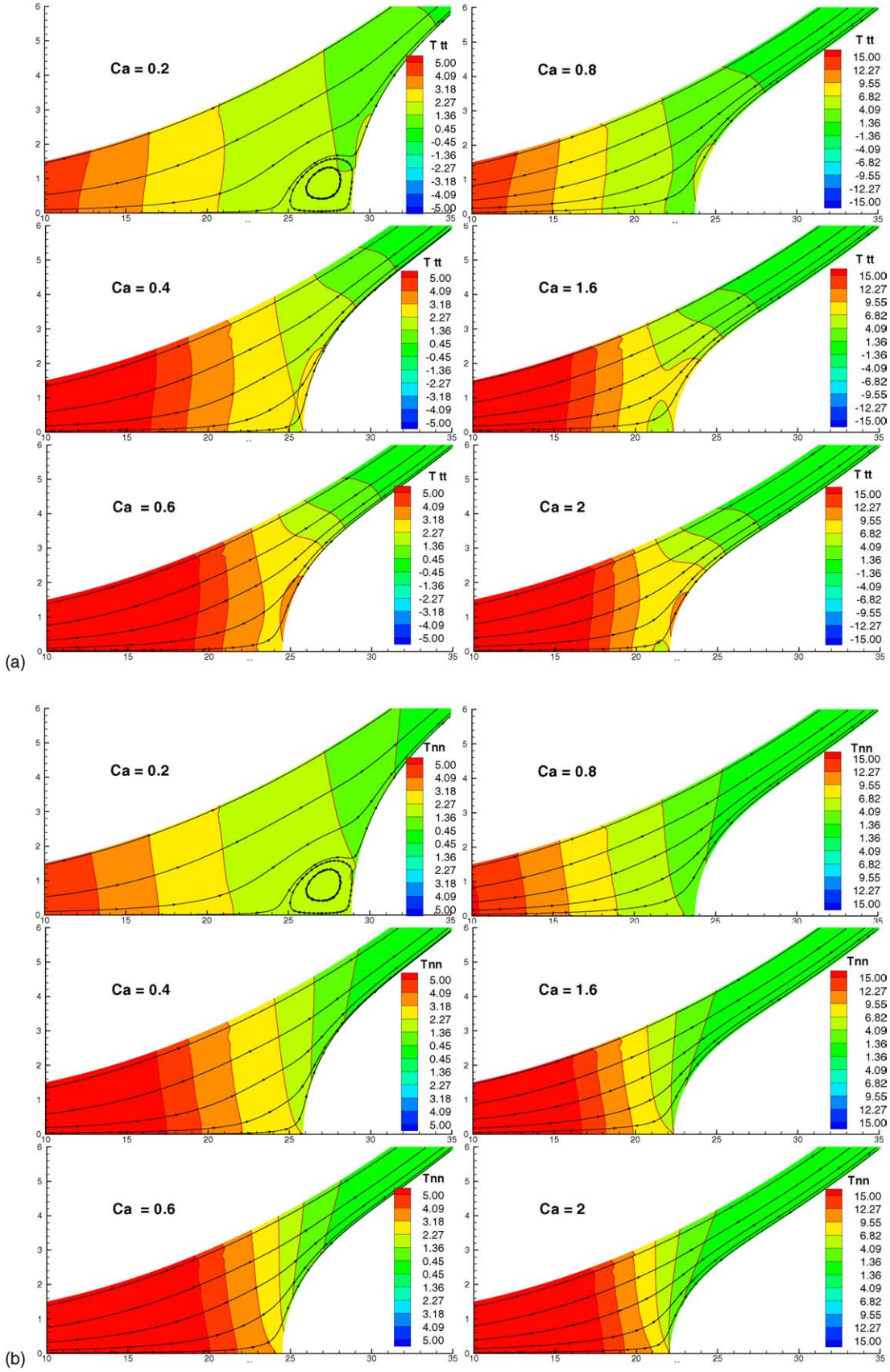

Fig. 7. Normal stress component along the streamlines. (a) T_{tt} and normal to the streamlines and (b) T_{nn} as a function of capillary number for Newtonian flow.

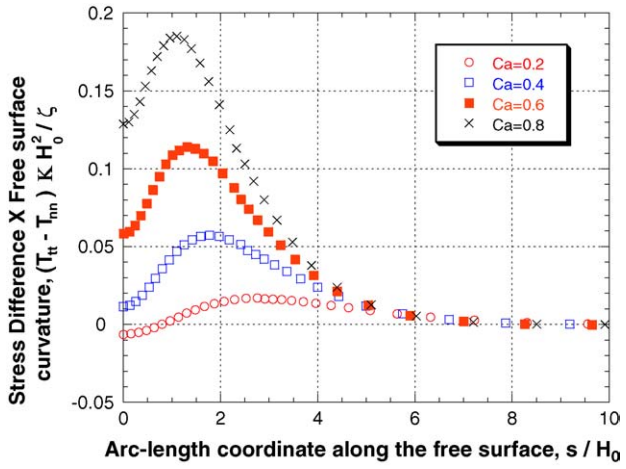

Fig. 8. Product of normal stress difference and local curvature along the free surface as a function of the capillary number.

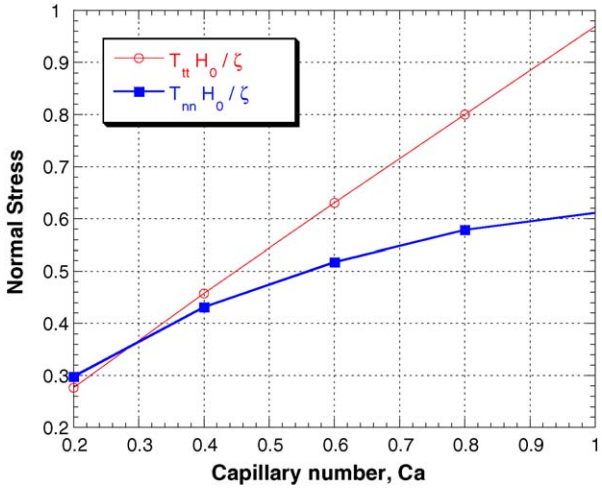

Fig. 9. Normal stresses along and perpendicular to the free surface at the film splitting stagnation point as a function of capillary number. The normal stress difference $T_{tt} - T_{nn}$ is the driving force for the flow instability that leads to ribbing.

shown in Fig. 6. Between $Ca = 0.6$ and 0.8, a strong transition takes place and the deformation rate at the free surface stagnation point rises considerably with capillary number. The critical capillary number at the onset of ribbing for Newtonian liquids predicted by linear stability analysis of the two-dimensional steady state flow at $H_0/R = 0.01$ is $Ca = 0.7$ [8,46].

The evolution of the normal stress components in the streamline direction T_{tt} and perpendicular to the streamlines T_{nn} near

Table 2
Meshes used in the study

Mesh	Elements	Degree of freedom	Max. *We* Old.-B	Max. *We* FENE-P
Mesh 1	1760	47391	3	3
Mesh 2	3960	105401	6	6
Mesh 3	7040	186291	8	11

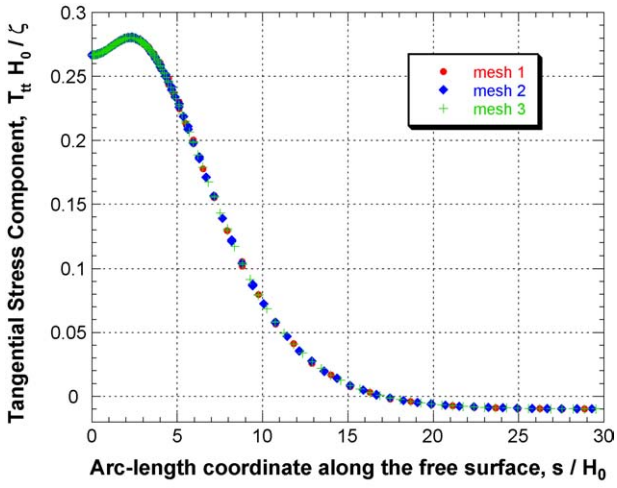

Fig. 11. Comparison of normal stress T_{tt} along the free surface using three different discretizations at $We = 3$, $Ca = 0.2$ and $b = 50$ (FENE-P model). The solutions are mesh independent.

the free surface as a function of capillary number is shown in Fig. 7. These normal stresses are a combination of pressure and normal viscous stress. At low capillary number, e.g., $Ca = 0.2$, the normal stress near the film split meniscus is weak. As the capillary number grows and the recirculation attached to the free surface disappears, the flow becomes stronger and the stresses at the meniscus rises considerably. The evolution of the product of the normal stress difference $T_{tt} - T_{nn}$ and the local curvature along the free surface as a function of the capillary number is shown in Fig. 8. $s = 0$ corresponds to the point at the symmetry line. According to Graham's analysis, this is the driving force for the meniscus instability. As the capillary number rises, the normal stress difference along the free surface becomes stronger. The high tangential stress at the film splitting stagnation point is related to the flow instability that leads to the formation of ribbing in forward roll coating at high capillary number.

Fig. 9 summarizes the evolution of the normal stress components T_{tt} (in the streamline direction) and T_{nn} (direction perpendicular to the streamlines) at intersection between the free surface and the symmetry line as the capillary number rises. At low

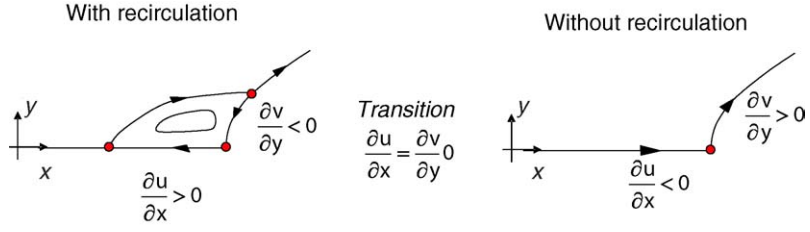

Fig. 10. Velocity gradient at different flow regimes, with and without recirculation attached to the free surface. The recirculation disappears when $\partial u/\partial x = \partial v/\partial y = 0$.

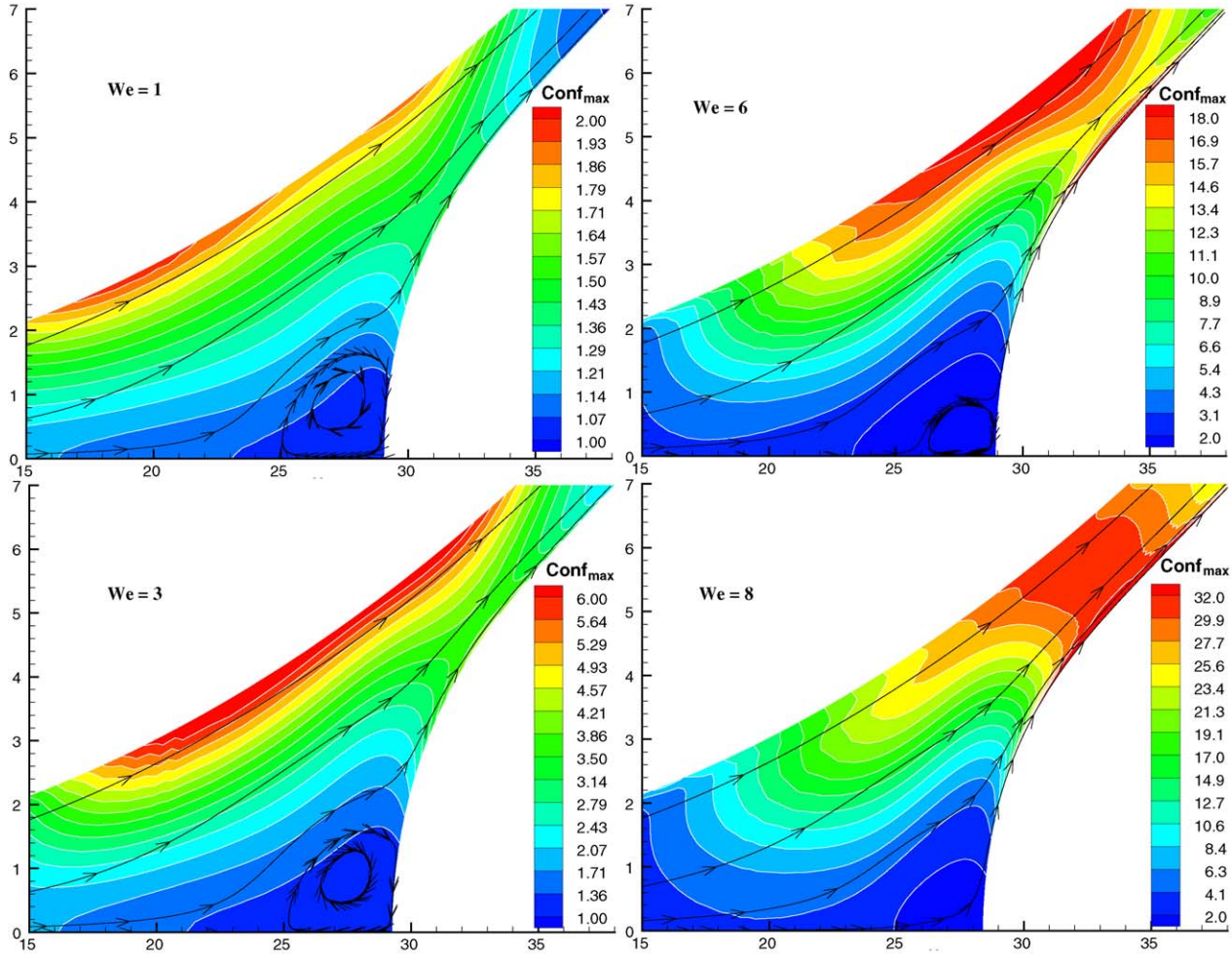

Fig. 12. Streamlines and maximum eigenvalue of the conformation tensor as a function of Weissenberg number at $Ca = 0.2$ (Oldroyd-B model).

capillary number, e.g. $Ca = 0.2$, there is a recirculation attached to the free surface at the separation point and $T_{nn} > T_{tt}$. As the capillary number increases, the normal stress on the streamline direction T_{tt} grows faster than the normal stress perpendicular to the free surface T_{nn}, and becomes larger than the latter at approximately $Ca \approx 0.3$. This flow state is the one at which the recirculation attached to the free surface disappears. As sketched in Fig. 10, when the recirculation is present, $\partial u/\partial x > 0$ and $\partial v/\partial y < 0$ at the intersection of the free surface and the symmetry line. When the flow has only one stagnation point at the symmetry line and no recirculation, $\partial u/\partial x < 0$ and $\partial v/\partial y > 0$. The transition occurs when $\partial u/\partial x = \partial v/\partial y = 0$ and consequently $T_{nn} = T_{tt} = -p$. The stress difference $(T_{tt} - T_{nn})$ at the symmetry line becomes stronger as the capillary number rises; this destabilizing force [1] leads to ribbing once it overcomes the stabilizing action of surface tension (in these operating conditions, linear stability analysis of the Newtonian flow predicts that ribbing occurs at $Ca \approx 0.7$).

3.2. Viscoelastic liquids

Viscoelastic free surface flows such as the one studied here present steep stress boundary layers attached to the free surface [24–26]. The stress boundary layer thins as Weissenberg number rises; therefore, for any given discretization there is a maximum value of the Weissenberg number above which the stress gradient cannot be resolved and the computation fails to converge. The maximum values of the Weissenberg number for all the three meshes tested and the two constitutive models used are reported in Table 2.

Fig. 11 shows the normal stress component T_{tt} along the film splitting meniscus at $We = 3$, $Ca = 0.2$ and $b = 50$ (FENE-P model) for the three different meshes tested.

The results show that the solutions obtained are mesh-converged. Most of the predictions presented hereafter were obtained with Mesh 3 in order to be able to achieve higher Weissenberg number.

The orthonormal eigenvectors $\mathbf{m_i}$ of the conformation dyadic $\mathbf{M}$ represent the three orthogonal directions along which molecules are stretched or contracted. The corresponding eigenvalues represent the square of the principal stretch ratios of flowing polymer segments, i.e., the average length square of polymer segments along the principal directions of stretch divided by the length square of the segments at equilibrium. The eigenvalues of $\mathbf{M}$ are always real and positive because the conformation tensor is symmetric and positive definite. Hereafter,

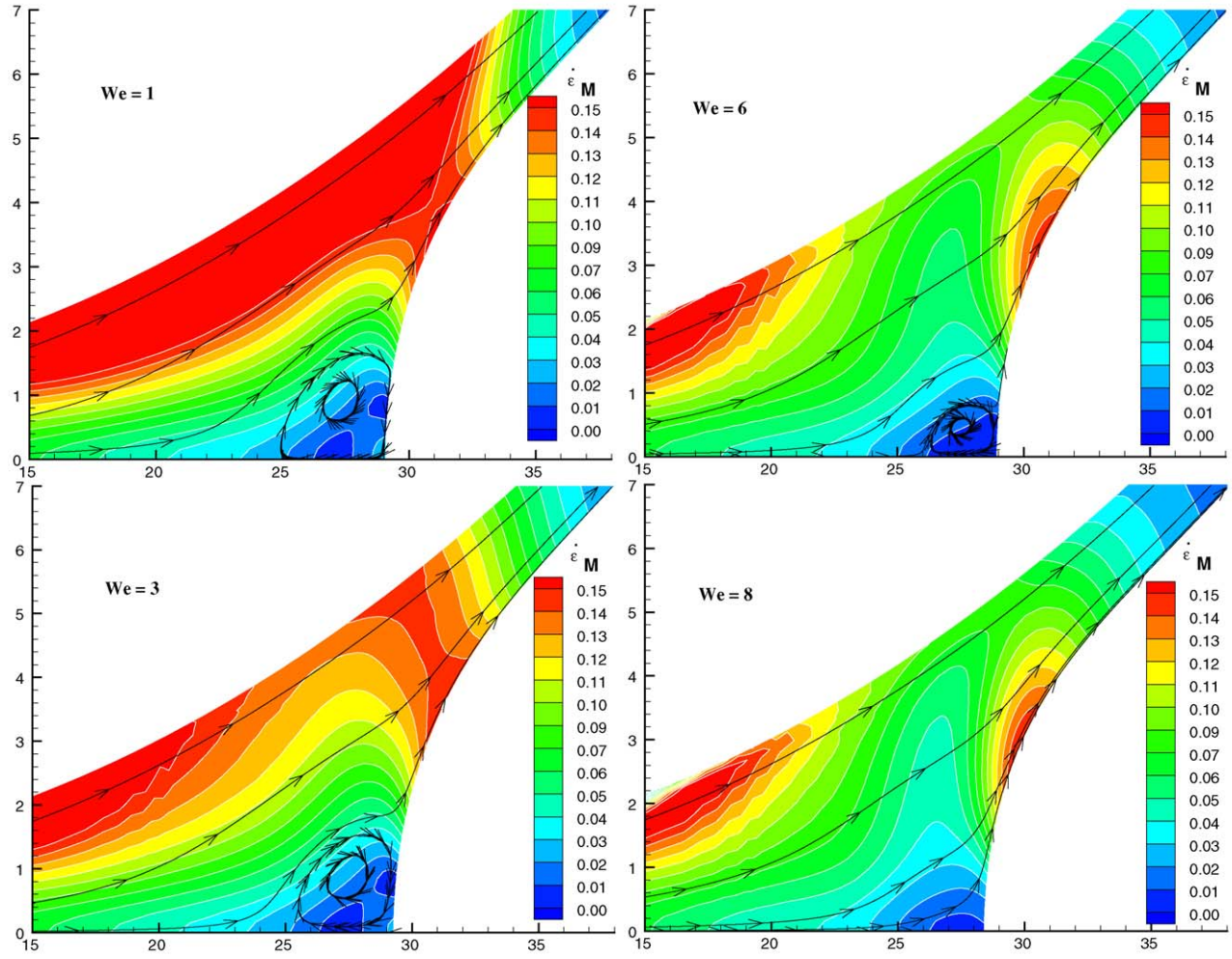

Fig. 13. Molecular extension rate near the free surface as a function of Weissenberg number at $Ca = 0.2$.

the convention is used $m_1 \leq m_2 \leq m_3$ to order the eigenvalues of conformation. The evolution of the streamlines and the maximum eigenvalue m_3 of the conformation dyadic as a function of the Weissenberg number at $Ca = 0.2$ obtained with the Oldroyd-B model is shown in Fig. 12. At $We = 1$, the flow is very close to that of a Newtonian liquid. There is a large recirculation attached to the free surface and the molecular extension is small ($m_3 < 2$). The highest molecular stretch occurs in the shear dominated flow near the roll surface. As the Weissenberg number rises, the polymer molecules become more and more stretched and a thin layer of high molecular extension grows at the free surface, downstream of the stagnation point. This region of high extension pulls liquid away from the recirculation and its size decreases as the Weissenberg number of the flow rises. At $We = 6$ the recirculation is much smaller than the one observed in Newtonian flow, and at $We = 8$ it has vanished. The elastic forces that come from the extended polymer molecules change completely the nature of the flow near the free surface. The flow at the film splitting stagnation point becomes much stronger as the elastic forces rise at a fixed capillary number.

The main difference between extensional and shear flows is that in extension polymer molecules are being extended along the preferred direction of stretch and orientation, and are being contracted along the direction where they are already contracted and least likely to be oriented, whereas in a shear flow the principal directions of stretching do not coincide with the principal directions of molecular orientation. Taking into account this important physical difference, Pasquali and Scriven [25] defined a mean ensemble molecular extension and shear rates

$$\dot{\varepsilon}_{\mathbf{M}} \equiv \mathbf{m}_3\mathbf{m}_3 : \mathbf{D}; \qquad \dot{\gamma}_{\mathbf{M}} \equiv |\mathbf{m}_1\mathbf{m}_3 : \mathbf{D}| \tag{12}$$

Fig. 13 shows the evolution of the molecular extension rate as a function of Weissenberg number at $Ca = 0.2$ (Oldroyd-B model). As expected, the deformation near the free surface is dominated by extension, and as the Weissenberg number rises, a region of high molecular extension is formed attached to the film splitting free surface just downstream of the stagnation point.

The strong extensional character of the flow near the free surface at high Weissenberg number leads to important changes in the stress field in that region. The evolution of the normal stress component of the stress tensor T_{tt} along the streamlines as a function of the Weissenberg number is shown in Fig. 14. At low capillary number, the stress field is similar to that of the Newtonian flow (see Fig. 7(a)). As the liquid elasticity grows,

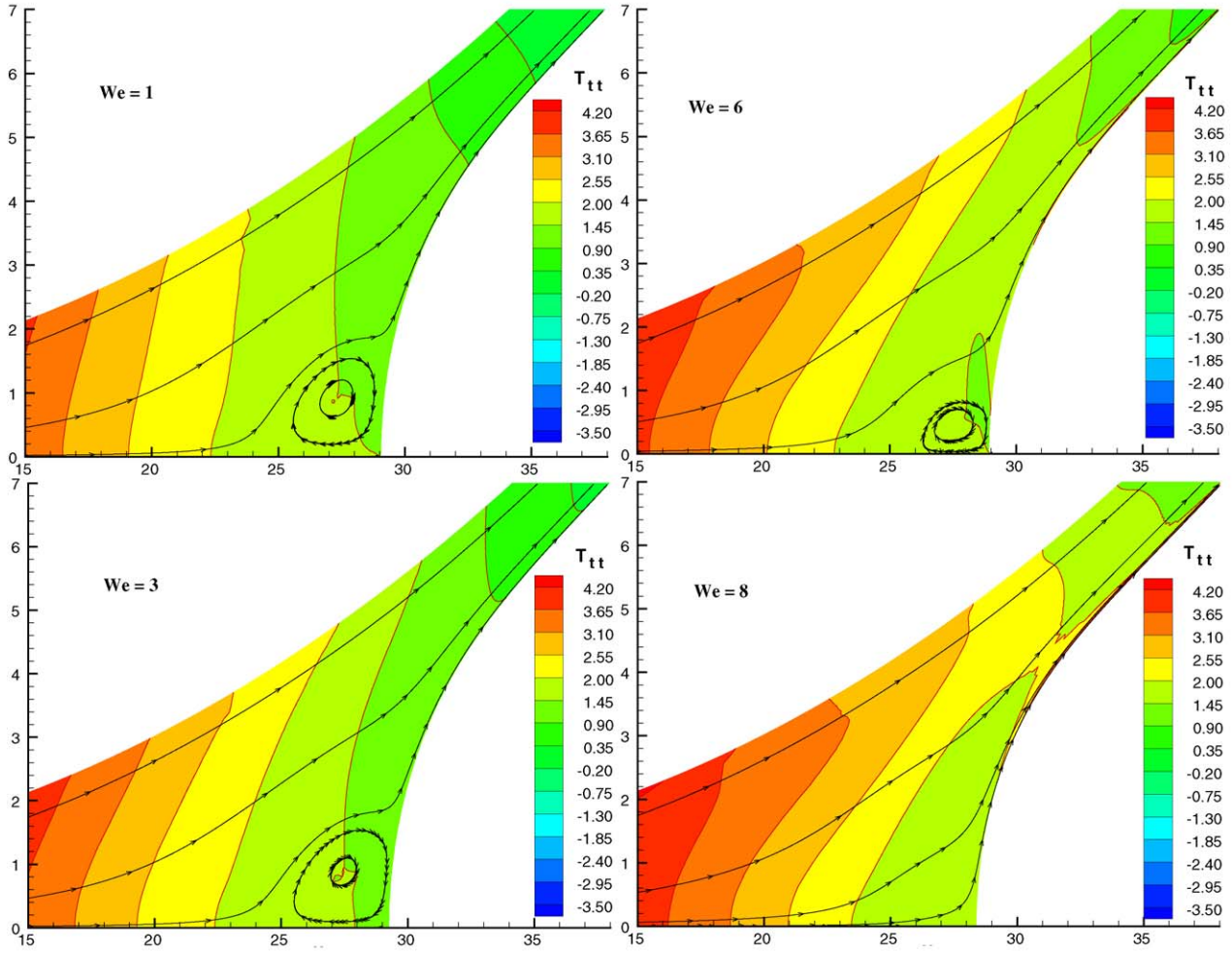

Fig. 14. Evolution of the normal stress component along the streamlines T_{tt} and streamlines as Weissenberg number grows. $Ca = 0.2$.

the constant stress bands are distorted in the direction of the main flow and the stress at the free surface rises. At high Weissenberg number, there is a high stress boundary layer attached to the free surface and the maximum value of the stress inside the boundary layer is a strong function of the Weissenberg number.

The evolution of the product of the normal stress difference $T_{tt} - T_{nn}$ and the local curvature along the free surface at $Ca = 0.4$ as a function of the Weissenberg number is presented in Fig. 15. This is the driving force for the flow instability. Interestingly, the highest value of the destabilizing force is not reached at the film-split location, but about one gap downstream of it.

Fig. 16 shows the evolution of the normal stresses along and perpendicular to the free surface, T_{tt} and T_{nn}, at the stagnation point located at the intersection of the symmetry line and the free surface as the Weissenberg number rises. The predictions shown were obtained with the Oldroyd-B model at $Ca = 0.2$. The Newtonian flow ($We = 0$) at this capillary number is stable with respect to three-dimensional perturbation, i.e. the stress difference $T_{tt} - T_{nn}$ is not strong enough to overcome the stabilizing action of surface tension. The normal stress perpendicular to the free surface T_{nn} is virtually independent of Weissenberg number. However, the normal stress along the streamlines T_{tt} grows as the liquid becomes more elastic. This effect is even stronger beyond the capillary number at which the recirculation attached to the free surface disappears. Clearly, the destabilizing stress difference $T_{tt} - T_{nn}$ grows as the liquid becomes more elastic. Therefore, at each capillary number, there is a critical

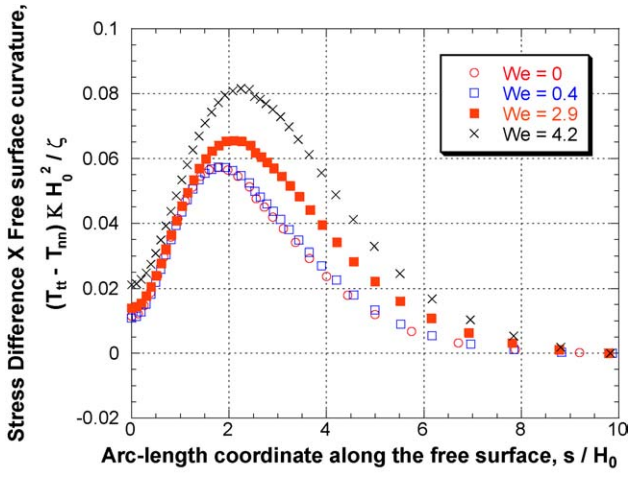

Fig. 15. Product of normal stress difference and local curvature along the free surface as a function of the Weissenberg number at $Ca = 0.4$.

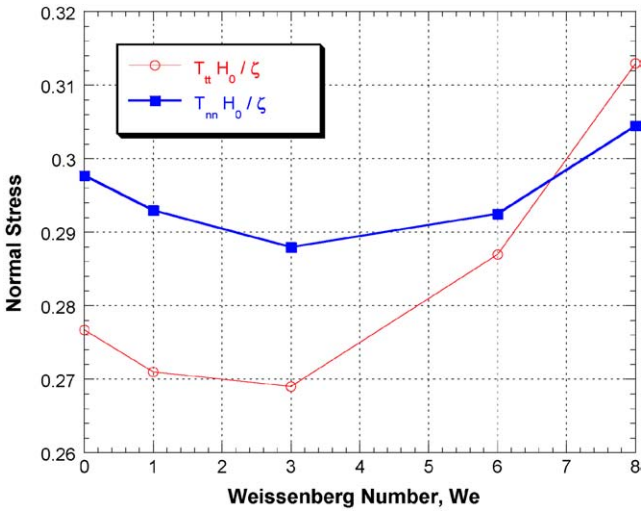

Fig. 16. Normal stresses along and perpendicular to the free surface at the film splitting stagnation point as a function of Weissenberg number at $Ca = 0.2$ (Oldroyd-B model). The normal stress difference $T_{tt} - T_{nn}$ is the driving force for the flow instability that leads to ribbing.

value of the Weissenberg number above which the normal stress difference along and perpendicular to the free surface becomes stronger than the stabilizing surface tension force and the flow becomes unstable with respect to cross-web disturbances.

All the predictions presented up to this point were obtained using the Oldroyd-B constitutive model, that assumes that the polymer molecules can be extended without bounds. This leads to unbounded extensional viscosity at finite extension rates. In the finitely extensible, non-linear elastic (FENE) constitutive equation, the maximum extensional of the molecules is finite and their rate of relaxation grows infinitely fast as the average molecular extension approaches its maximum value. The parameter b, defined as the ratio of the maximum length square of the polymer molecules to their average length square at equilibrium, controls the molecular extensibility. The effect of the polymer extensibility is analyzed next. As the molecules becomes stiffer, i.e., b falls, the maximum elastic stress decreases, as expected. Fig. 17 shows the tangential and normal components of the polymeric stress σ_{tt} and σ_{nn} at $Ca = 2$, $We = 2$ and different values of b. The predictions obtained at $b = 100$ (not shown) virtually coincide with those obtained with the Oldroyd-B model.

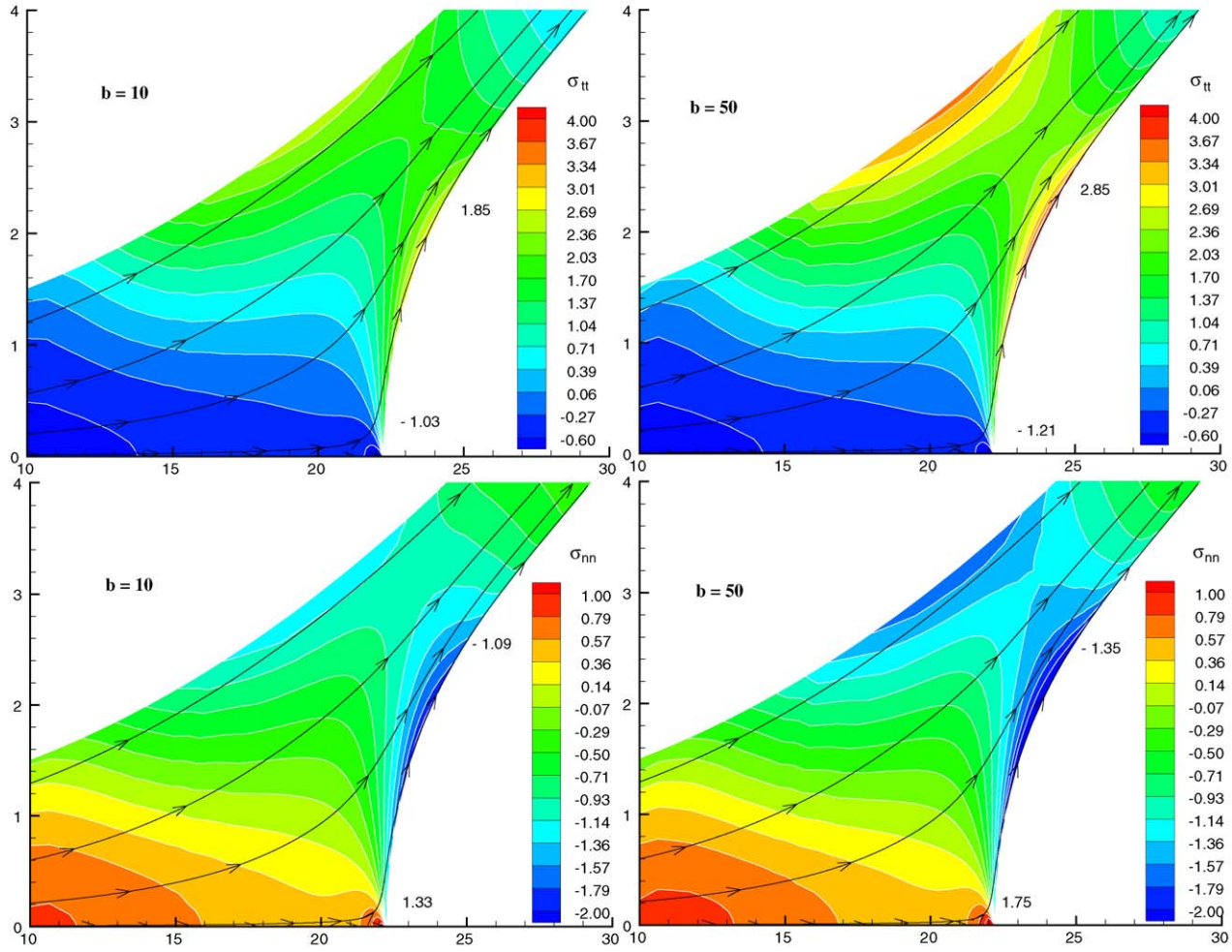

Fig. 17. Normal components of the elastic stress normal (σ_{nn}) and tangential (σ_{tt}) to the streamlines as a function of molecular extensibility b for $Ca = 2$ and $We = 2$ (FENE-P model).

4. Conclusion

In forward roll coating, above a critical capillary number, the two-dimensional film splitting meniscus becomes three-dimensional, resulting in more or less regular stripes in the coated liquid film. For Newtonian liquids, the stability of the two-dimensional flow is determined by a competition of surface tension and viscous forces. Several experimental studies have shown that liquid viscoelasticity destabilizes the flow. When minute amounts of flexible polymer are present, the onset of the three-dimensional instability occurs at much lower speeds than in the Newtonian case. The mechanisms responsible for this early onset of the instability are not completely understood yet.

The two-dimensional flow of viscoelastic liquids in a forward roll coating gap was analyzed by solving the continuity and momentum equations coupled with two differential constitutive equations, the Oldroyd-B and FENE-P models. The resulting set of differential equations was solved by weighted residual method and finite element basis functions. The predictions reported here describe the mechanisms by which liquid elasticity destabilizes the flow: the extensional flow downstream of the film splitting stagnation point leads to a high elastic stress at the free surface. This high stress in the streamline direction pulls liquid away from the recirculation that is present in Newtonian flows at low capillary number. As the recirculation diminishes and ultimately disappears, the flow near the stagnation point becomes stronger and the elastic stresses at the meniscus even higher. Consequently, the normal stress difference acting on the free surface grows with Weissenberg number; this is the driving force of the instability that leads to the formation of ribbing [1]. At any given capillary number, there is a critical Weissenberg number above which the flow becomes unstable.

Acknowledgements

This work was funded by CNPq (Brazilian Research Council), by the National Science Foundation of the U.S.A. (CTS-CAREER-0134389 and CTS-ITR-0312764) and by gifts from ExxonMobil and 3M Corporation. The Center for Biological and Environmental Nanotechnology supported by the NSF Nanoscale Science and Engineering Initiative (EEC-0118007) is gratefully acknowledged for providing the supercomputing resources for the most intensive computations.

References

[1] M.D. Graham, Interfacial hoop stress and instability of viscoelastic free surface flows, Phys. Fluids 15 (2003) 1702–1710.
[2] J.R.A. Pearson, The stability of uniform viscous flow under rollers and spreaders, J. Fluid Mech. 7 (1960) 481–500.
[3] E. Pitts, J. Greiller, The flow of thin liquid films between rollers, J. Fluid Mech. 11 (1961) 33–50.
[4] C.C. Mill, G.R. South, Formation of ribs on rotating rollers, J. Fluid Mech. 28 (1967) 523–529.
[5] J. Greener, T. Sullivan, B. Turner, S. Middleman, Ribbing instability of a two-roller coater: Newtonian fluids, Chem. Eng. Comm. 5 (1980) 73–83.
[6] M. Savage, Mathematical model for the onset of ribbing, AIChE J. 30 (1984) 999–1002.
[7] H. Benkreira, M.F. Edwards, W. Wilkinson, Ribbing instability in the roll coating of Newtonian fluids, Plastic Rubber Proc. Appl. 2 (1982) 137–144.
[8] D.J. Coyle, C.W. Macosko, L.E. Scriven, Stability of symmetrical film-splitting between counter- rotating cylinders, J. Fluid Mech. 216 (1990) 437–458.
[9] D.J. Coyle, C.W. Macosko, L.E. Scriven, Film-splitting flows of shear-thinning liquids in forward roll coating, AIChE J. 33 (1987) 741–746.
[10] T. Bauman, T. Sullivan, S. Middleman, Ribbing instability in coating flows-effect of polymer additives, Chem. Eng. Comm. 14 (1982) 35–46.
[11] J.E. Glass, Dynamics of roll spatter and tracking. 1. Commercial latex trade paints, J. Coat. Technol. 50 (1978) 53–60.
[12] J.E. Glass, Dynamics of roll spatter and tracking. 2. Formulation effects in experimental paints, J. Coat. Technol. 50 (1978) 61–68.
[13] J.E. Glass, Dynamics of roll spatter and tracking. 3. Importance of extensional viscosities, J. Coat. Technol. 50 (1978) 56–71.
[14] J.E. Glass, Dynamics of roll spatter and tracking. 4. Importance of G-star recovery and N1 in tacking, J. Coat. Technol. 50 (1978) 72–78.
[15] D.A. Soules, R.H. Fernando, J.E. Glass, Dynamic uniaxial extensional viscosity (DUEV) effects in roll application. 1. Rib and web growth in commercial coatings, J. Rheol. 32 (1988) 181–198.
[16] R.H. Fernando, J.E. Glass, Dynamic uniaxial extensional viscosity (DUEV) effects in roll application. 2. Polymer blend studies, J. Rheol. 32 (1988) 199–213.
[17] M.S. Carvalho, T.J. Anderson, L.E. Scriven, Ribbing instability in forward deformable roll coating, Proceedings of the 1994 TAPPI Coating Conference, 1994, pp. 99–104.
[18] P. Dontula, Polymer solutions in coating flows, Ph.D. thesis, University of Minnesota, Minneapolis, MN, available from UMI, Ann Arbor, MI, order number 9937847, 1999.
[19] A.M. Grillet, A.G. Lee, E.S.G. Shaqfeh, Observations of ribbing instabilities in elastic fluid flows with gravity stabilization, J. Fluid Mech. 399 (1999) 49–83.
[20] F. Varela Lopez, L. Pauchard, M. Rosen, M. Rabaud, Non-Newtonian effects on ribbing instability threshold, J. Non-Newton. Fluid Mech. 103 (2002) 123–139.
[21] M.D. Graham, Theory of viscoelastic free surface flow instability, Proceedings of the 74th Annual Meeting of the Society of Rheology, Minneapolis, MN, USA, October 2002.
[22] K.N. Christodoulou, L.E. Scriven, Finding leading modes of a viscous free surface flow: an asymmetric generalized eigenproblem, J. Sci. Comput. 3 (1988) 355–385.
[23] M.S. Carvalho, L.E. Scriven, Three-dimensional stability analysis of free surface flows: application to forward deformable roll coating, J. Comp. Phys. 151 (1999) 534–562.
[24] M. Pasquali, Polymer molecules in free surface coating flows, Ph.D. thesis, University of Minnesota, Minneapolis, MN, available from UMI, Ann Arbor, MI, order number 9963019, 2000.
[25] M. Pasquali, L.E. Scriven, Free surface flows of polymer solutions with models based on the conformation tensor, J. Non-Newton. Fluid Mech 108 (2002) 363–409.
[26] A.G. Lee, E.S.G. Shaqfeh, B. Khomami, A study of viscoelastic free surface flows by the finite element method: Hele–Shaw and slot coating flows, J. Non-Newton. Fluid Mech. 108 (2002) 327–362.
[27] Y. Dimakopoulos, J. Tsamopoulos, On the gas-penetration in straight tubes completely filled with a viscoelastic fluid, J. Non-Newton. Fluid Mech. 117 (2004) 117–139.
[28] B. Sadanandan, R. Sureshkumar, Numerical eigenspectrum of non-viscometric viscoelastic flows: results for the periodic channel flow, J. Non-Newton. Fluid Mech. 108 (2002) 143–161.
[29] M.D. Smith, Y.L. Joo, R.C. Armstrong, R.A. Brown, Linear stability analysis of flow of an Oldroyd-b fluid through a linear array of cylinders, J. Non-Newton. Fluid Mech. 109 (2003) 13–50.
[30] K.N. Christodoulou, Computational physics of slide coating flow, Ph.D. thesis, University of Minnesota, Minneapolis, MN, available from UMI, Ann Arbor, MI, order number 9021329, 1990.

[31] J.M. de Santos, Two-phase cocurrent downflow through constricted passages, Ph.D. thesis, University of Minnesota, Minneapolis, MN, available from UMI, Ann Arbor, MI, order number 9119386, 1991.
[32] P.A. Sackinger, P.R. Schunk, R.R. Rao, A Newton-Raphson pseudo-solid domain mapping technique for free and moving boundary problems: a finite element implementation, J. Comp. Phys. 125 (1996) 83–103.
[33] M.S. Carvalho, L.E. Scriven, Flows in forward deformable roll coating gaps: comparison between spring and plane strain model of roll cover, J. Comp. Phys. 138 (1997) 449–479.
[34] A.N. Beris, B.J. Edwards, Thermodynamics of Flowing Systems with Internal Microstructure, first ed., Oxford University Press, Oxford, 1994.
[35] R.J.J. Jongschaap, K.H. de Haas, C.A.J. Damen, A generic matrix representation of configuration tensor rheological models, J. Rheol. 38 (1994) 769–796.
[36] M. Pasquali, L.E. Scriven, Theoretical modeling of microstructured liquids: a simple thermodynamic approach, J. Non-Newton. Fluid Mech 120 (2004) 101–135.
[37] Y. Kwon, A.I. Leonov, Stability constraints in the formulation of viscoelastic constitutive equations, J. Non-Newton. Fluid Mech. 58 (1995) 25–46.
[38] R.A. Bird, C.F. Curtiss, R.C. Armstrong, O. Hassager, Dynamics of Polymeric Liquids, second ed., vol. 2, John Wiley & Sons, New York, 1987.
[39] X. Xie, M. Pasquali, A new, convenient way of imposing open-flow boundary conditions in two- and three-dimensional viscoelastic flows, J. Non-Newton. Fluid Mech. 122 (2004) 159–176.
[40] M.S. Carvalho, Roll coating flows in rigid and deformable gaps, Ph.D. thesis, University of Minnesota, Minneapolis, MN, available from UMI, Ann Arbor, MI, order number 9621887, 1996.
[41] S.F. Kistler, L.E. Scriven, Coating flows, in: J.R.A. Pearson, S.M. Richardson (Eds.), Computational Analysis of Polymer Processing, Applied Science Publishers, London, 1983, pp. 243–299.
[42] S.F. Kistler, L.E. Scriven, Coating flow theory by finite element and asymptotic analysis of the navier-stokes system, Int. J. Numer. Methods Fluid. 4 (1984) 207–229.
[43] K.N. Christodoulou, L.E. Scriven, Discretization of free surface flows and other moving boundary problems, J. Comp. Phys. 99 (1992) 39–55.
[44] V.F. de Almeida, Domain deformation mapping: application to variational mesh generation, SIAM J. Sci. Comput. 20 (1999) 1252–1275.
[45] R.A. Cairncross, P.R. Schunk, T.A. Baer, R.R. Rao, P.A. Sackinger, A finite element method for free surface flows of incompressible fluids in three dimensions. Part I. Boundary fitted mesh motion, Int. J. Numer. Methods Fluids 33 (2000) 375–403.
[46] M.S. Carvalho, L.E. Scriven, Deformable roll coating flows: steady state and linear perturbation analysis, J. Fluid Mech. 339 (1997) 143–172.
[47] R. Guenette, M. Fortin, A new finite element method for computing viscoelastic flows, J. Non-Newton. Fluid Mech. 60 (1995) 27–52.
[48] M.J. Szady, T.R. Salamon, A.W. Liu, R.C. Armstrong, R.A. Brown, A new mixed finite element method for viscoelastic flows governed by differential constitutive equations, J. Non-Newton. Fluid Mech. 59 (1995) 215–243.
[49] H.B. Keller, Numerical solution of bifurcation and nonlinear eigenvalue problems, in: P. Rabinowitz (Ed.), Applications of Bifurcation Theory, Academic Press, NY, 1977, pp. 359–384.
[50] J.H. Bolstad, H.B. Keller, A multigrid continuation method for elliptic problems with folds, SIAM J. Sci. Stat. Comput. 7 (1985) 1081–1104.
[51] H.B. Keller, The bordering algorithm and path following near singular points of higher nullity, SIAM J. Stat. Comput. 4 (1983) 573–582.